Semiconductor Metal Oxides Doped with Gold Nanoparticles for Use in Acetone Gas Sensors

Semiconductor Metal Oxides Doped with Gold Nanoparticles for Use in Acetone Gas Sensors

E. Ovodok[1], V. Kormosh[2], V. Bilanych[3], M. Ivanovskaya[1]

[1]Laboratory of Thin Films Chemistry of Research Institute for Physical Chemical Problems of the Belarusian State University, Minsk 220006, Republic of Belarus
[2]Institute of Analytical Technique of Uzhhorod National University, Uzhhorod 88000, Ukraine
[3]Department of Applied Physics, Uzhhorod National University, Uzhhorod 88000, Ukraine

E-mail address: vbilanych@gmail.com

Abstract. The effect of nanosized gold particles on the adsorption-sensitive properties of SnO_2–Au sensors under the detection of acetone vapors has been studied. Different techniques for the preparation of SnO_2–Au nanocomposites with an average Au particle size of 2 nm were applied. It has been found that a fivefold increase in the sensor response to acetone vapors and threshold sensitivity (C_{lim}) of 0.1 ppm are achieved by adding gold to tin dioxide in the colloidal form during synthesis. While adding gold in ion form (Au (III)) leads to a growth of the sensor response to acetone vapors by 2.7 times and defines C_{lim} of 0.2 ppm. The slope of the calibration curves of the SnO_2–Au sensors allows registering acetone vapors at concentrations ranging from C_{lim} to 5 ppm. This concentration range can be used for express diagnostics in diabetes. The enhanced sensitivity of SnO_2–Au sensors to acetone vapors can be explained by an increase in the adsorption–catalytic activity of tin ions as a result of the modifying effect of sulfate groups and the envolving of highly dispersed gold in the adsorption – catalytic process of oxidation of acetone molecules.

1. Introduction

To diagnose various diseases and monitor the health status of patients with certain chronic illnesses, different methods to identify markers (substances accompanying these diseases in the human body) are used [1, 2]. In particular, the possibilities of determining some markers in human exhale in dental diseases and diabetes are being widely studied [3, 4]. Many of these biomarker substances are present in the exhale of a healthy person, but their concentration increases in case of a disease.

When diagnosing diabetes, acetone vapors are determined in the exhale of a person, since the concentration of other substances is considerably lower. Different methods for determining acetone vapors are being developed. In recent years, along with the most common method of chromatography (gas chromatography with a plasma photometric detector (PPD)), intensive work is underway to establish the possibility of determining acetone vapors using sensors [5]. Metal oxide resistive sensors are predominantly studied among different types of sensors [5]. An intensive experimental work has been carried out to test different metal oxide materials as acetone sensors [5, 6]. The interest in these

type of sensors is caused by the fact that this might be a new area of their application. The research being carried out should show how this direction will be applicable in the practice of express diagnostics.

The search for promising materials for acetone vapors sensors is carried out mainly empirically. Different types of oxide materials doped with activating additives have been tested [5–7]. It was shown that the most promising are WO_3 and ZnO-based materials. However, other semiconducting metal oxides may also be applicable. SnO_2 is a traditional and widely used material in the production of gas sensors for toxic and flammable gases. It is suitable for the machine technology of sensor manufacturing. Tin dioxide is characterized by high thermal and chemical stability and has a wide band gap of 3.6 eV. The gas sensitivity of SnO_2-based sensors is significantly improved when doped with different additives [8, 9].

Nanosized oxide materials are used for acetone sensors. Different methods for the synthesis of nanosized metal oxides have been developed. This allows obtaining particles with different morphology: rods, bars, sticks, threads, fibers, tubes, thin sheets and strips, flowers, petals, porous structures, etc. All these anisotropic particles with the size ranging from 120–500 nm to 1–2 μm consist of small isotropic particles, the diameter of which corresponds to the nanometer range (less than 100 nm). Various organic additives are used in the synthesis of anisotropic nanoparticles of metal oxides (citrate ions, dimethylformamide, pluronic, PVP, surfactants). Such syntheses are carried out in an ethanol/H_2O mixture by the template or carbon-thermal method. The presence of C-containing substances not only promotes the growth of particles of a given shape, but also contributes to the formation of an oxide structure with a high concentration of structural defects. Partial reduction of oxides leads to the formation of oxygen vacancies and ions with a lower than the main oxidation state. In addition, synthesis with carbon-containing additives promotes the formation of metastable phases of metal oxides (WO_3, In_2O_3, ZnO), which may have the adsorption and conductive properties different from that of the stable phases [5–7]. However, the influence of these factors remains poorly studied. It is known that the highest sensitivity threshold (0.007–0.067 ppm) to acetone vapors is achieved by doping SnO_2 with carbon and nitrogen [8, 9].

In the synthesis of SnO_2 materials for acetone sensors, $SnCl_4$ or $SnCl_2$ are most often used as precursors. Although it is known that using other tin salts makes it possible to exclude the negative effect of chloride ion impurities on the adsorption-catalytic properties of SnO_2-sensors. The modifying effect of sulfate ions on the surface state of different metal oxides is known. Sulfate ions improve their catalytic properties in oxidation reactions [10–13].

This work is aimed at the study of the effect of the nanoscale gold particles on the gas sensitivity of the SnO_2–Au nanocomposites to acetone vapors. A distinctive feature of the studied SnO_2–Au nanocomposites is that both components (SnO_2, Au) are nanosized. Tin dioxide was synthesized via $SnSO_4$ as a starting material according to the previously developed technique that allows obtaining nanosized tin dioxide particles with surface modified by sulfate groups [11].

2. Materials and experiments

2.1. Methods of synthesis

Tin dioxide (SnO_2) was synthesized by sol-gel method via $SnSO_4$ salt. The synthesis technique includes a preliminary treatment of $SnSO_4$ (20 g) with 20 ml of H_2SO_4 (98 wt. %) under heating at 200 °C for 10 min. At the end of the reaction, the solution was diluted with distilled water up to 200 ml. Then, ammonia solution (5 vol. %) was added dropwise until pH 8 was reached. The obtained precipitate was separated by a centrifugation and washed 3 times with distilled water. Next, 50 ml of distilled water and 0.1 ml of sulfuric acid (98 wt. %) were added to the precipitate. The suspension was ultrasonicated (f = 22 kHz, P = 130 W) for 2 minutes and $SnO_2 \cdot nH_2O$ sol was prepared. According to the TEM analysis, after heating $SnO_2 \cdot nH_2O$ xerogel at 600 °C, SnO_2 powder was obtained with a narrow particle size distribution and average diameter $d \approx 5.5$ nm [10–12].

The SnO_2–Au nanocomposites were obtained by adding the colloid solution of gold or $HAuCl_4$ solution into $SnO_2 \cdot nH_2O$ sol in the quantity corresponding to 0.15 at. % of Au relative to SnO_2. The

formation of SnO_2–Au nanocomposite occurs under thermal treatment of hydroxylated amorphous tin oxide containing nanosized Au particles or Au ions, respectively.

To obtain the colloidal solution of gold, $AuCl_4^-$ ions were reduced by sodium borohydride in the presence of 5-(2-mercaptoethyl) tetrazole stabilizer [14]. The Au particles size in a colloidal solution was 1.9 ± 0.1 nm. Au particles retain their size when added to SnO_2–Au nanocomposite. The sample obtained using the gold colloidal solution is denoted as **SnO_2–Au^0**.

No gold particles were detected by TEM method in SnO_2–Au nanocomposites obtained by adding Au (III) into the $SnO_2 \cdot nH_2O$ sol. This can be explained by both the small size and the specific morphology of the gold particles. According to the XPS data presented below, the gold content on the surface of this sample is 5 times lower than the amount added into the sol during synthesis and constitutes 0.03 at. %. This result may indicate an encapsulation of Au particles with tin dioxide under conditions of joint formation of the SnO_2–Au nanocomposite from a colloidal solution of SnO_2 nH_2O + Au ^{III} during thermal dehydration. The optical spectra of such composite allows suggesting that the gold particles are about 2 nm in size. This sample is denoted as **SnO_2–Au^{III}**.

Table 1. The samples studied in this paper

Sensing material	Au state	Stabilizer of Au nanoparticles	d_{Au}, nm
SnO_2	–	–	–
SnO_2–Au^0	nanoparticles	5-(2-mercaptoethyl)-tetrazole	1.9 ± 0.1
SnO_2–Au^{III}	$HAuCl_4$	–	~2

2.2. Methods of characterization

The samples were characterized by transmission electron microscopy (TEM), infrared (IR) spectroscopy, X-ray photoelectron spectroscopy (XPS) and UV-Vis spectroscopy. The grain size distribution was ascertained on a LEO-906E transmission electron microscope. The IR-spectra were recorded on an AVATAR-330 (Thermo Nicolet) spectrometer equipped with a Smart Diffuse Reflectance accessory in the wavelength range of 400–4000 cm^{-1}. The XPS spectra were measured from the surface of the original samples. XPS signals were recorded using a Thermo Scientific K-Alpha XPS system (Thermo Fisher Scientific Inc., UK) equipped with a microfocused monochromatic Al *K*α X-ray source (1486.68 eV). UV-Vis absorption spectra were recorded using a Shimadzu UV-2550 spectrophotometer.

2.3. Manufacturing the sensors and measuring their characteristics

To manufacture the sensing elements, the SnO_2 and SnO_2–Au powders were ground thoroughly in ethanol to obtain the corresponding pastes. The pastes were used to form thick-film layers on microplatforms for sensors. The general view of the sensor and sensing element is depicted in Fig. 1. The thickness of the sensitive layer was about 150 μm.

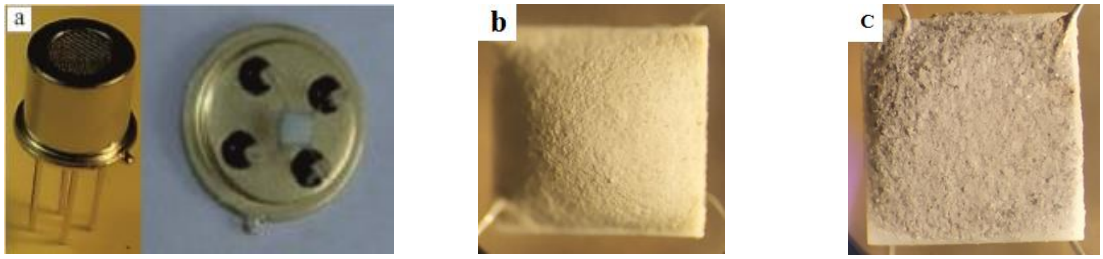

Figure 1. Photographs of the sensor (a) and sensing element of SnO_2 (b) and SnO_2–Au^{III} (c)

The standard microplatforms made of aluminium oxide substrates with platinum heater and measuring electrodes were used. The microplatform width was 1.6 mm and thickness was 0.25 mm (Fig. 2). The sensing elements were mounted in a standard casing (see Fig. 1, a). The resistance of the sensors in wet air (R_0) and standard acetone-air mixtures (R_g) were measured in a constant voltage mode. The temperature-dependent responses of the sensors were mainly acquired at 50 ppm of acetone vapors.

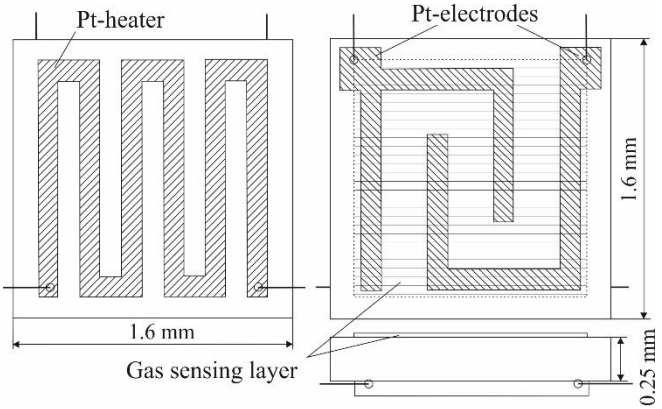

Figure 2. Scheme of the microplatform with measuring electrodes and heater

3. Results and discussions

3.1. Gas-sensing properties

The dependence of the sensor response on the working temperature when detecting 50 ppm acetone vapors are presented in Fig. 3. Adding gold into the nanocomposites leads to a significant growth of the output signal of the SnO_2-based sensors. The response increases by 5 times in case of SnO_2–Au^0 sensors and by 2.7 times in case of SnO_2 –Au^{III} sensors in comparison with SnO_2 sensors. The optimal temperature range for the detection of acetone vapors is at higher temperature for sensors containing gold particles. Effective acetone detection is observed for these sensors in the range from 300 to 390 ºC with a maximum at 340–370 ºC. The wide temperature range of acetone vapors detection maight indicate the implementation of an additional and more effective detection mechanism on the surface of the SnO_2–Au sensors in comparison with the SnO_2 sensor.

Dynamic parameters can indicate different mechanisms of acetone detection by SnO_2–Au^0 sensor. Figure 4 shows the dependences of the sensor responses to 10 ppm of acetone vapors vs time. The response time measured for SnO_2–Au sensors is short enough (3–6 s). Recovery to 70 % of initial parameters of SnO_2–Au^0 sensors, after the end of the gas supply, occurs quickly, and then it slows down and becomes as slow as for SnO_2 sensors. This may indicate the difficulty in the desorption of acetone molecules or products of its oxidation. The changes in the electrical characteristics of SnO_2–Au^0 sensors can be described by two of the known mechanisms: the direct adsorption–desorption of volatile organic compounds on the SnO_2 surface [7, 15] and oxidation–reduction, the so-called “oxygen vacancy model”. [16]. It was found that acetone molecules are adsorbed at SnO_2 surface on tin ions by the oxygen of the carbonyl group with the transfer of electron density to the oxide [15, 17]. The intermediate and final products of the adsorption of ketones on oxides have been studied [18]. Surface acetate is the most common product of ketones chemisorption on oxides surfaces at 350 ˚C [17, 19].

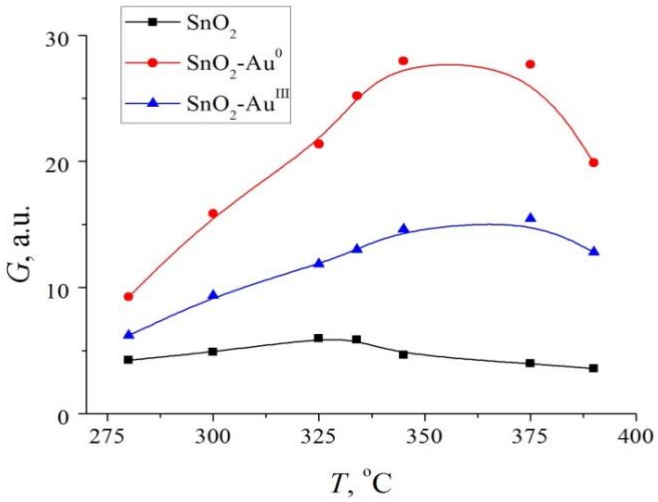

Figure 3. The sensor response vs working temperature graphs of the SnO_2, SnO_2–Au^{III}, and SnO_2–Au^0 sensors under detection of acetone vapors (50 ppm)

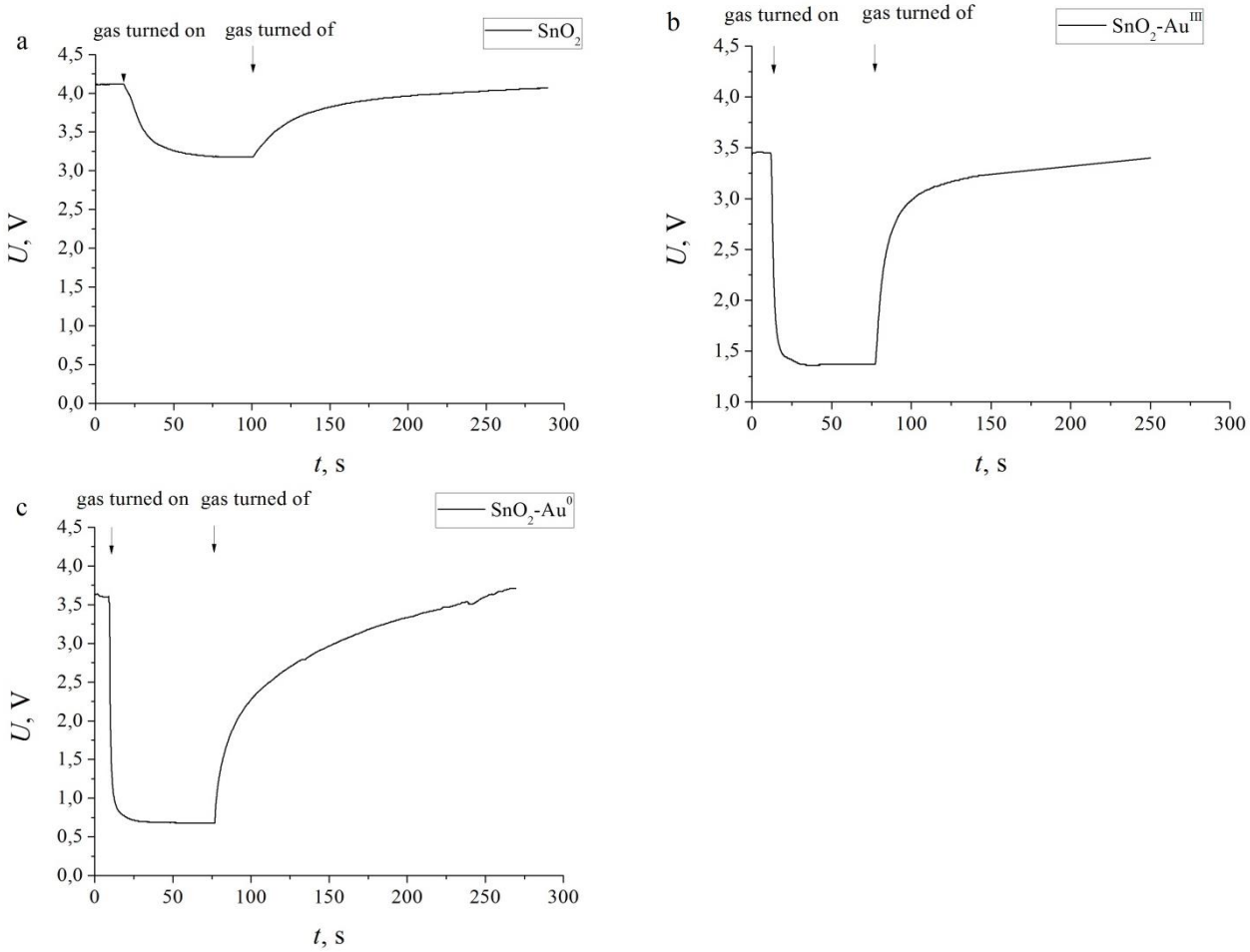

Figure 4. Dynamic characteristics of the SnO_2(a), SnO_2–Au^{III}(b), and SnO_2–Au^0(c) sensors under detection of acetone vapors (10 ppm)

The study of sensors for the determination of low concentrations of acetone vapors (less than 5 ppm) deserves special attention. This range can be used for express diagnosis of diabetes. As it is known, the acetone content is 0.3–0.9 ppm in the exhale of a healthy person. The acetone concentration in the exhale may grow up to 1.8–5.0 ppm for a person with diabetes. Fig. 5 shows the dependences of the response of the sensors on the concentration of acetone vapors. The slope of the curve for SnO_2–Au sensors allows distinguishing between small changes in acetone vapors concentration from a minimal detectable value up to 5 ppm. SnO_2 sensor does not possess such possibility.

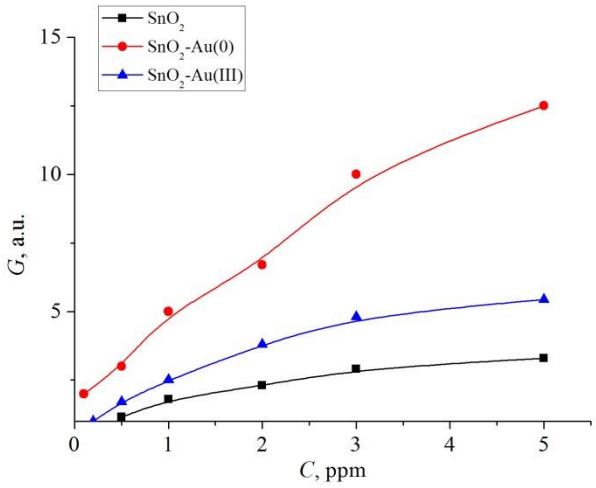

Figure 5. Dependences of the response of SnO_2, SnO_2–Au^0, and SnO_2–Au^{III} sensors on the concentration of acetone vapors

3.2. Structural features

A significant difference in the properties of the SnO_2–Au^0 and SnO_2–Au^{III} sensors is observed. The structural features of these nanocomposites are considered to explain the differences in the properties of the sensors. The structural characteristics of these nanocomposites were studied in details in our previous work [12]. The states of Au and the surface of SnO_2 in SnO_2–Au^0 and SnO_2–Au^{III} nanocomposites are presented in Table 1. Some results on the study of the samples by XPS, Auger, and IR spectroscopy methods are also presented.

Table 2. Structural features of SnO_2–Au samples. Full results are given in [12].

Sample	Au, at %, (XPS)	BE, eV Au $4f_{5/2}$	α = BE Sn $3d_{5/2}$ + KE Sn MNN (XPS)	BE, eV S 2*p*	S–O (IR)
SnO_2–Au^0 0.15 at %	0.12	84.0 (Au^0)	SnO_2, Sn^{2+} impurity [SnO_5V_o]	169.3 SO_4^{2-}	SO_4^{2-}, bident. SO_3^{2-}, monodent.
SnO_2–Au^{III} 0.15 at %	0.03	83.9 (Au^0) 84.9 Au^+Au_n)	SnO_2	169.3 SO_4^{2-}	SO_4^{2-}, bident

According to the XPS data, the gold content on the surface of the SnO_2–Au samples is different. The amount of 0.12 at. % was found in SnO_2–Au^0 sample and 0.03 at. % – in SnO_2–Au^{III} sample. The Au 4*f* and Au 3*d* lines in the spectra of SnO_2–Au^0 and SnO_2–Au^{III} samples have low intensity and large width (FWHM $3d_{5/2}$ ~ 4 eV), which is a result of small size of gold particles. The shape of the Au $4f_{7/2}$ and Au $4d_{5/2}$ lines with maxima at 84.0 ±0.1 and 335.2 ±0.1 eV indicates the occurrence of Au^0 state in the

SnO_2–Au^0 sample. In the XPS spectrum of SnO_2–Au^{III} sample, the Au $4d_{5/2}$ line is hardly distinguishable whereas two Au $4f_{7/2}$ peaks of low intensity with BE =83.9 and 84.9 eV are registered. The first peak corresponds to Au^0 state. The second one can be attributed to Au^+ state [20]. Thermal treatment at 600 °C should have evoked the complete transformation of Au(III) ions to the metal state of gold (Au^0). However, this conversion might be hindered in $SnO_2 \cdot nH_2O$ + Au(III) amorphous system resulting in the stabilization of the partially oxidized state of gold on the surface of the gold clusters – $(Au_n)Au^+$.

A slight shift in the position of the maximum of the Sn $3d_{5/2}$ line at 487.3 ± 0.1 eV towards lower binding energies in the spectrum of SnO_2–Au^0 sample may be caused by imperfection of its structure, caused by the appearance of oxygen vacancies [SnO_5V_o] in the environment of tin cations [21]. A large oxygen deficiency may cause the appearance of Sn^{2+} cations in SnO_2 structure [22].

The modified Sn Auger parameter (α = BE Sn $3d_{5/2}$ + KE Sn MNN AES) [20] is a more reliable indicator of tin state. The measured value of this parameter indicates the occurrence of SnO_2 phase in SnO_2 and SnO_2–Au^{III} samples. Also, it does not exclude Sn^{2+} admixture occurred in SnO_2–Au^0 sample.

The S 2*p* peak o with BE ≈169.3 eV attributed to SO_4^{2-} ion is registered in the XPS spectra of the samples [23]. The sulphur content was estimated on the surface of the samples to be 2.7–3.1 at. %.

IR spectroscopic data confirm the presence of SO_x-groups in the samples. Bidentate bound sulfate groups SO_4^{2-} predominate [24]. The line at 820 cm^{-1} in the spectrum of SnO_2–Au^0 sample can be an attribute of the monodentate O-coordinated SO_3 group on SnO_2 surface. Annealing the samples at 600 °C also promotes the formation of sulfate groups on the surface of tin dioxide.

The presence of sulfate-sulfite groups in the samples can be explained by the adsorption of SO_2 on SnO_2 surface. Sulphate ions, included in SnO_2 nH_2O sol from precursors ($SnSO_4$, H_2SO_4), are source of SO_2. In the case of SnO_2–Au^0 sample, the S-containing stabilizer of Au colloidal particles 5-(2-mercaptoethyl)tetrazole is an additional source of SO_2. Thermal destruction of this substance occurs in stages [25]. A large amount of gaseous products is formed as a result of the destruction of the tetrazole ring. Sulfur removal occurs at the last stage (500–600 °C). These factors have a significant effect on the formation of the crystal structure and surface of Au and SnO_2 particles from amorphous $SnO_2 \cdot nH_2O$ xerogel. These factors also explain the appearance of structural defects, primarily oxygen vacancies and Sn^{2+} cations in the SnO_2–Au^0 sample, since structural oxygen from $SnO_2 \cdot nH_2O$ and SnO_2 can take part in the oxidation of the stabilizer of Au colloidal particles. Disordered fragments of tin dioxide structure (Sn_nO_{2n-1}) as well as the Au/Sn_nO_{2n-1} boundaries can act as oxygen activation centers.

It is known [13,26,27] that the adsorbed forms of SO_2 change the nature of active centers on the surface of metal oxides. They increase the strength of Lewis acid sites (surface metal ions) due to the induction effect. The induction effect consists in the shift of the electron density from tin cations by SO_2 molecules.

Thus, two factors – the defectiveness of the SnO_{2-x} structure and the presence of adsorbed forms of SO_2 allows explaining the high sensitivity of SnO_2–Au^0 sensors to acetone vapors. The higher response of the SnO_2–Au^0 sensors as compared to the SnO_2–Au^{III} sensors is explained by the high defectiveness of the SnO_2 surface and the high concentration of Au on their surface.

Table 2 shows some parameters of the sensors studied in this work in comparison with other SnO_2 sensors. In the selected tin dioxide sensors, the synthesis of the sensitive material was carried out using carbon-containing organic substances and polymers. The sensors based on SnO_2 without dopants and doped with Au are discussed in [28,29]. For comparison, SnO_2 sensors doped with Ru or Rh [30,31] are considered. Ruthenium, like gold, is a catalyst for the partial oxidation of organic substances. The catalytic activity of rhodium is poorly studied. The PdAu/SnO_2 sensor with a bimetallic additive is characterized by the highest sensitivity threshold to acetone vapors among the SnO_2 sensors doped with noble metals [32].

The SnO_2–Au nanocomposites investigated in this work differ from the materials listed in Table 2 by the smallest sizes of SnO_2 and Au particles, as well as by a low concentration of gold. However, they are highly sensitive to low concentrations of acetone vapors. The threshold sensitivity of SnO_2–Au^0 sensors is comparable to that of PdAu/SnO_2 sensor. This bimetallic sensor is characterized by a

synergistic effect that increases their sensitivity. Other sensors (Au–SnO_2; Au/SnO_2; Rh–SnO_2; Ru–SnO_2) have a lower threshold sensitivity to acetone.

Table 3. Comparison of the properties of some acetone sensors

Material	Morphology	C_{Lim}, ppm	Temp. °C	$S=R_o/R_g$, 50 ppm	Type of sensor	Ref.
SnO_2	*NP, d_{SnO2} = 4–6 nm	0.5	320	6	Planar electrode substrate	This paper
SnO_2–Au	NP, d_{SnO2} = 4–6 nm d_{Au} = 1.9 nm	0.1	340	30	Planar electrode substrate	This paper
SnO_2–Au^{III},	NP, d_{SnO2} = 4–6 nm d_{Au} = 2 nm	0.2	340	16	Planar electrode substrate	This paper
SnO_2	Multichannel **NFs d = 150–250 nm		310	11.4	Alumina substrate	[28]
SnO_2 Au–SnO_2	Hollow micro-spheres 600–900 nm d_{SnO2} = 20–50 nm	- 5	280 220	- 30	Ceramic tube	[29]
SnO_2 Rh-SnO_2	NFs d=150 nm d_{SnO2} = 6–10 nm	- 1	200 200	6 60	Planar electrode substrate	[30]
SnO_2 Ru-SnO_2	NFs d = 120–150 nm d_{SnO2} = 6–9 nm	5 0.5	200 200	4 40	Planar electrode substrate	[31]
SnO_2 Au/SnO_2 Pd/SnO_2 PdAu/SnO_2	Nanospheres, d_{SnO2} = 7–12 nm,| d_{Au} = 3–10 nm	 5 - 0.1	290 280 250 250	12 71 42 109	Ceramic tube	[32]

The response of SnO_2–Au^0 sensor is comparable or less than that of other Au-SnO_2 sensors when detecting 50 ppm acetone This can be explained by the lower content of Au (0.15 at % or 0.2 wt %.) in SnO_2–Au^0 than in other sensors with higher response – Au/SnO_2, PdAu/SnO_2 (0.9507 %) [33], Rh–SnO_2 (0.5 mol. % Rh) [31], Ru–SnO_2 (2 mol. % Ru) [32].

4. Conclusions

Adding colloidal gold with a particle size of 1.9 ± 0.1 nm, stabilized by 5-(2-mercaptoethyl) tetrazole, into the SnO_2 nH_2O sol enhances the sensitivity of the SnO_2–Au^0 sensors to low concentrations of acetone vapors. The threshold sensitivity of SnO_2–Au^0 sensors to acetone is 0.1 ppm.

The slope of the concentration curve of SnO_2–Au^0 sensors allows detecting acetone concentrations in the range from 0.1 ppm to 5 ppm, which is necessary for the express diagnosis of diabetes.

The high sensitivity of SnO_2–Au sensors to acetone vapors is due to the effect of SO^{4-} groups on the adsorption activity of SnO_2 surface and the evolving of highly dispersed Au in the oxidation process of acetone molecules.

Acknowledgments

This work was performed within the framework of an international Ukrainian-Belarusian grant (Belarusian RFFR grants No. X21UKRG-002).

References

[1] D. Hill, R. Binions 2012 *Inter. journal on smart sensing and intelligent systems* **5** (2) 401 https://doi.org/10.21307/ijssis-2017-488
[2] B. Buszewski, M. Kesy, T. Ligor and A. Amann 2007 *Biomed. Chromatogr.* **21** 553 https://doi.org/10.1002/bmc.835
[3] V. Saasa, T Malwela , M Beukes, M. Mokgotho, Ch-Pu Liu and B. Mwakikunga 2018 *Diagnostics* **8** 12 https://doi.org/10.3390/diagnostics8010012
[4] M. Righettoni, A. Tricoli 2011 *J. Breath. Res.* **5** 037109 https://doi.org/10.1088/1752-7155/5/3/037109
[5] M. Masikini, M. Chowdhury, and O. Nemraoui 2020 *J. Electrochem. Soc.* **167** 037537 https://doi.org/10.1149/1945-7111/ab64bc
[6] N. Alizadeh, H. Jamalabadi, F. Tavoli 2020 *IEEE Sensors Journal* **20** (1) 5 https://doi.org/10.1109/JSEN.2019.2942693
[7] S. Americo, E. Pargoletti, R. Soave, F. Cargnoni, M. I. Trioni, G. L. Chiarello, G. Cerrato, G. Cappelletti 2020 *Electrochimica Acta* **371** 137611 https://doi.org/10.1016/j.electacta.2020.137611
[8] J. Hu, C. Zou, Y. Su, M. Li, Z. Yang, M. Ge, Y. Zhang 2017 *Sens. Actuators B Chem.* **253** 641 https://doi.org/10.1016/j.snb.2017.06.176
[9] X. Guan, Y. Wang, P. Luo, Y. Yu, D. Chen, and X. Li. 2019 *Nanomaterials* **9** (3), 445 https://doi.org/10.3390/nano9030445
[10] E. Ovodok, M. Ivanovskaya, D. Kotsikau, V. Kormosh, I. Alyakshev 2015 *Physics, Chemistry and Applications of Nanostructures* 313 https://doi.org/10.1142/9789814696524_0078
[11] E. Ovodok, M. Ivanovskaya, D. Kotsikau, V. Kormosh, P. Pylyp, V. Bilanych 2021 U*krainian Journal of Physics* **66** (9) 803 https://doi.org/10.15407/ujpe66.9.803
[12] M. Ivanovskaya, E. Ovodok, T. Gaevskaya, D. Kotsikau, V. Kormosh, V. Bilanych, M. Micusik 2021 *Materials Chemistry and Physics* **258** 123858 https://doi.org/10.1016/j.matchemphys.2020.123858
[13] L.M. Kustov, V.B. Kazansky, F. Figueras, D. Tichit 1994 *J. Catal.* **150** 143 https://doi.org/10.1006/jcat.1994.1330
[14] C. Guhrenz, A. Wolf, M. Adam, L. Sonntag, S.V. Voitekhovich, S. Kaskel, N. Gaponik, A. Eychmüller 2017 *Z. Phys. Chem.* **231** 51 https://doi.org/10.1515/zpch-2016-0879
[15] A. A. Abokifa, K. Haddad, J. Fortner, C. S. Lo, P. Biswas 2018 *J. Mater. Chem. A* **6** 2053 https://doi.org/10.1039/C7TA09535J
[16] A. Tricoli, M. Righettoni, A. Teleki 2010 *Angew. Chem. Int. Ed.* **49** 7632 https://doi.org/10.1002/anie.200903801
[17] W. Thoren, D. Kohl and G. Heiland 1985 *Surface Sci.* **162** (1-3) 402 https://doi.org/10.1016/0039-6028(85)90927-6
[18] P. G. Harrison, B. M. Maunder 1984 *J. Chem. Soc., Faraday Trans. I* **80** 1329 https://doi.org/10.1039/F19848001329
[19] A.-K. Elger, C. Hess 2019 *Angew. Chem. Int. Ed.* **58** 15057 https://doi.org/10.1002/anie.201908871
[20] Practical surface analysis by Auger and X-ray photoelectron spectroscopy. Edited by D. Briggs and M. P. Seah. John Wiley and Sons Ltd. Chichester. 1983.
[21] Y. Yang, Y. Wang, S. Yin 2017 *Appl. Surf. Sci.* **420** 399 https://doi.org/10.1016/j.apsusc.2017.05.176
[22] S. Shi, D. Gao, Q. Xu, Z. Yang, D. Xue 2014 *RSC Advances* 4 (85) 45467 https://doi.org/10.1039/C4RA05475J
[23] C.L. Lau, G.K. Wertheim 1978 *J. Vac. Sci. Technol.* (15) 622 https://doi.org/10.1116/1.569642
[24] K. Nakamoto 1986 Infrared and Raman spectra of inorganic and coordination compounds. John Wiley & Sons, Ltd.
[25] S.V. Voitekhovich, A. Wolf, C. Guhrenz, A.S. Lyakhov, L.S. Ivashkevich, M. Adam, N. Gaponik, S. Kaskel, A. Eychmueller, 2016 *Chem. Eur J.* **22** 14746 https://doi.org/10.1002/chem.201602980

[26] F. Berger, E. Beche, R. Berjoan, D. Klein, A. Chambaudet 1996 *Appl. Surf. Sci.* **93** 9 https://doi.org/10.1016/0169-4332(95)00319-3
[27] M.A. Babaeva, A.A. Tsyganenko, V.N. Filimonov 1984 *Kinetics and Catalysis* **25** (4) 787
[28] T. Wang, S. Ma, L. Cheng, X. Jiang, M. Zhang, W. Li, W. Jin 2016 *Materials Letters* **164** 56 https://doi.org/10.1016/j.matlet.2015.10.118
[29] Y. Li, L. Qiao, D. Yan, L. Wang, Y. Zeng, H. Yang 2014 *Journal of Alloys and Compounds* **586** 399 https://doi.org/10.1016/j.jallcom.2013.09.147
[30] X. Kou, N. Xie, F. Chen, T. Wang, L. Guo, C. Wang, Q. Wang, J. Ma, Y. Sun, H. Zhang, and G. Lu 2018 *Sensors and Actuators B: Chemical* **256** 861 https://doi.org/10.1016/j.snb.2017.10.011
[31] X. Kou, F. Meng, K. Chen, T. Wang, P. Sun, F. Liu, X. Yan, Y. Sun, F. Liu, K. Shimanoe, and G. Lu 2020 *Sensors and Actuators B: Chemical* **320** 128292 https://doi.org/10.1016/j.snb.2020.128292
[32] G. Li, Z. Cheng, Q. Xiang, L. Yan, X. Wang, and J. Xu, 2019 *Sensors and Actuators B: Chemical* **283** 590 https://doi.org/10.1016/j.snb.2018.09.117